RF plasma-enhanced conducting Polymer/W_5O_{14} based self-propelled micromotors for miRNA detection

Gamze Celik Cogal [a,1], Gozde Yurdabak Karaca [a,b,1], Emre Uygun [c], Filiz Kuralay [d], Lutfi Oksuz [e], Maja Remskar [f], Aysegul Uygun Oksuz [a,*]

[a] Department of Chemistry, Faculty of Arts and Sciences, Suleyman Demirel University, Isparta, Turkey
[b] Department of Bioengineering, Faculty of Engineering, Suleyman Demirel University, Isparta, Turkey
[c] Department of Civil Engineering, Faculty of Engineering, Suleyman Demirel University, Isparta, Turkey
[d] Department of Chemistry, Faculty of Science, Hacettepe University, Ankara, Turkey
[e] Department of Physics, Faculty of Arts and Sciences, Suleyman Demirel University, Isparta, Turkey
[f] Solid State Physics Department, Jozef Stefan Institute, Ljubljana, Slovenia

HIGHLIGHTS

- Micromotor application of W_5O_{14} microwires was presented for the first time.
- RF-Rotating plasma PEDOT modified W_5O_{14} microwires were successfully synthesized.
- SsDNA probe immobilized micromotors detected miRNA-21 sensitively and selectively.
- The speed and fluorescence intensities of micromotors changed with hybrization.
- These micromotors can facilitated early cancer diagnosis.

GRAPHICAL ABSTRACT
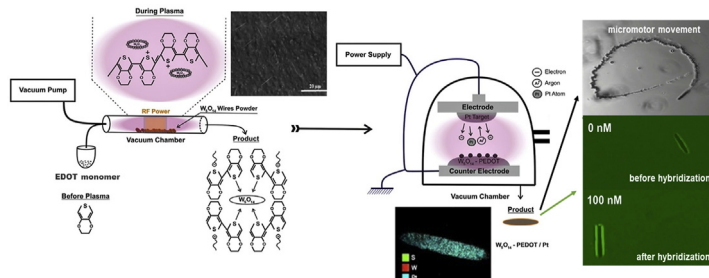
ARTICLE INFO

ABSTRACT

Functionalized micro/nanomotors having immobilized biological molecules provide excellent and powerful tools for the detection of target molecules. Based on surface modifications and mobilities of micromotors, we report herein a new experimental design of high-speed, self-propelled and plasma modified micromotors for biomedical applications. Within this scope, in the first step, poly (3,4-ethylenedioxythiophene) (PEDOT) was in-situ synthesized onto W_5O_{14} (tungsten trioxide) wires by using radio frequency (RF) rotating plasma reactor. Then, W_5O_{14}/PEDOT-Platinum (Pt) hybrid micromotors were fabricated by using magnetron sputtering technique. The detection of miRNA-21 was performed using both single-stranded DNA (ssDNA) (probe DNA) immobilized W_5O_{14}—Pt and W_5O_{14}/PEDOT-Pt micromotors. The fluorescence signals were determined after hybridization of probe DNA immobilized these novel W_5O_{14}—Pt and W_5O_{14}/PEDOT-Pt micromotors with different molar concentrations of the synthetic target (6-carboxyfluorescein dye (FAM)-labeled miRNA-21). The changes in the micromotor speeds after the hybridization process were also evaluated. W_5O_{14}/PEDOT-Pt micromotors presented better sensor properties compared to the W_5O_{14}—Pt micromotors. A good linearity for miRNA-21 concentration between 0.1 nM and 100 nM was obtained for these micromotors based on their fluorescence intensities. The detection limit was found as 0.028 nM for W_5O_{14}/PEDOT-Pt micromotors

---

* Corresponding author.
  E-mail address: ayseguluygun@sdu.edu.tr (A.U. Oksuz).
[1] GCC and GYK made equal contributions.

(n = 3). Thus, sensor and motor characteristics of the W_5O_{14}–Pt micromotors were improved by RF plasma enhanced PEDOT coatings. The new catalytic W_5O_{14} based micromotors demonstrated here had great potential for the development of sensitive and simple sensing platforms for detection of miRNA-21.

1. Introduction

Inspired by the biomachines of nature, scientists have devoted remarkable efforts to the development of artificial micro/nanoscale motors similar to the macroscopic ones present in our everyday life. Micro/nanomotors represent a primary step towards the realization of convenient nanomachines. Nano-, micro-, and macroscopic level of the synthetic motors are designed in order to obtain a mechanical motion such as cargo transport [1] and object translocation. One example of such promising artificial machines are synthetic nano/micromotors, which are small devices that can perform self-propelled motion in fluids by converting different types of energies into mechanical movement [2]. Nano/micromotors have metallic parts, which play a role as catalysts to decompose of hydrogen peroxide to the products of water and oxygen gas. The bubbles of oxygen gas trigger the propulsion of the motors [3,4]. For example, catalytic decomposition of hydrogen peroxide (H_2O_2) has been frequently reported for the propulsion of synthetic nano/micromotors including nanowire motors [5–10].

The movement of man-made micromachines provides benefits for biomedical fields such as drug delivery, diverse environmental and biomedical applications and sensing [11,12]. Among various biomedical applications of the nano/micromotors, early cancer detection has become a priority due to the fact that cancer is one of the most serious deadly diseases that kills millions of people nowadays [13]. Because of the importance of early cancer diagnosis and the need to differentiate multiple cancers, studies have focused on identifying and validating microRNA (miRNA) signatures. To date, giant range of miRNAs have been identified in animals, plants, microorganisms and over 4000 miRNAs have been defined in humans [14,15]. miRNAs are small (18–25 nt in length), single-stranded, endogenous and non-protein-coding RNA molecules that control the expression of target genes [16]. In addition to their effective use in neurological and autoimmune diseases, miRNAs are specific markers for various types of cancers due to variations in miRNA expression levels [17,18]. Particularly, miRNA-21 is an important biomarker used for mainly breast, prostate, colorectal and lung cancers diagnosis [17–19]. Therefore, there is an urgent need to develop sensitive and selective methods for miRNA-21 detection. Esteban-Fernandez de Avila et al. produced ultrasound-driven dye-labeled single-stranded DNA (ssDNA)/graphene-oxide (GO) coated gold nanowires (AuNWs) based motor system for miRNA recognition. They showed that these nanomotors recognized the cancer cell based on the endogenous content of the target miRNA in the presence of miRNA-21 expression in MCF-7 and HeLa cells [20]. Such nanomotor-based biosensing approach leads to ways to monitor miRNA expression at the single-cell level, promoting the investigation of miRNA in clinical applications.

In the current work, we aimed to design new micromotor system including inorganic/organic hybrid systems for detection of miRNA-21. N-type semiconductor tungsten trioxide structures are extremely important among many semiconductor oxide nano/micromaterials because of their low cost, non-toxicity, high efficiency and biocompatibility [21]. The combination of biological molecules and metal oxides plays an important role in the development of nano/microscale devices in the field of clinical diagnosis

and treatment [22]. A good sensitivity (26.56 Ω ng^{-1} mL cm^{-2}) and a wide linear detection range (1–250 ng mL^{-1}) for cardiac troponin I (cTnI) detecting 3-aminopropyl triethoxysilane (APTES) conjugated tungsten trioxide nanoparticles (APTES/n-WO_3) were introduced by Sandil et al. [23]. Shuai et al. fabricated a WO_3-graphene composite, exhibiting significant sensing performance for miRNA with a detection limit of 0.05 fM [24].

W_5O_{14} compound belongs to the W_nO_{3n-1} Magneli's phases and has favorable properties in comparison with other tungsten oxide phases [25]. Various number of reports have been published to investigate the properties of tungsten-based materials for different applications. However, the production of tungsten-based nanomaterials with better morphologies is still a challenge for highly sensitive sensor applications. This work describes a novel sensitive method using W_5O_{14} wire-based micromotor approach for miRNA-21 detection. W_5O_{14} nanowires were modified with PEDOT using RF rotating plasma polymerization method. W_5O_{14}/Pt and W_5O_{14}/PEDOT-Pt microwires were prepared by RF magnetron sputtering coating method. Among many conducting polymers, poly (3,4-ethylenedioxythiophene) (PEDOT) has attracted great attention due to its lightweight, conductivity, mechanical flexibility, unique chemical and redox properties, along with minimal structural defects, high aqueous stability and biocompability [26–29]. Because of these properties, functionalized-polymer microstructures play an important role for various biomedical applications such as micro/nanoscale actuators, drug carriers or metabolite and genetic biosensors [30–32].

In the present work, the changes in the fluorescence intensity as well as the changes in the speed of W_5O_{14}/Pt and W_5O_{14}/PEDOT-Pt micromotors were examined before and after hybridization of the probe DNA immobilized onto micromotors with target miRNA-21. Analytical signals based on speeds and distances were the basis of the motion-oriented DNA detection approach. These motors can be also capture various nucleic acids instantly with a high sensitivity and selectivity [33,34]. The propulsion of the micromotor was performed in the presence of 3% H_2O_2 fuel (containing 5% of the Triton X-100 surfactant). The prepared micromotors demonstrated long life time, excellent bubble propulsion motion which can be detected even in the presence of low concentration of hydrogen peroxide. To the best of our knowledge, this study is the first to present preparation of W_5O_{14}/Pt and W_5O_{14}/PEDOT-Pt micromotors and their applications for cancer biomarker detection. Due to active motion characteristics as well as their certain functional properties such as easy conjugation with biomolecules, the functionalized micromotors can identify the hybridization process sensitively and efficiently.

2. Experimental

2.1. Reagents and solutions

Platinum targets from China Leadmat Advanced Materials Co. LTD (2 inch diameter and 0.25 inch thickness) were used for magnetron sputtering process. Hydrogen peroxide (H_2O_2) (30%), sodium hydroxide (NaOH), 3,4-ethylenedioxythiophene (EDOT), bovine serum albumin, Tris-HCl and ethylenediamine tetraacetic

acid (EDTA) were purchased from Sigma-Aldrich. Triton X-100 was purchased from Fluka. Other chemicals were from Sigma-Aldrich. All chemicals used were of analytical-grade quality. Synthetic oligonucleotides were purchased from Heliks Biotechnology (Turkey). miRNA-21 plays a significant role in the development of breast cancer, not by promoting or inhibiting tumor occurrence directly, but rather by binding to complementary sequences within the 3′UTR (three prime untranslated region) of target miRNA transcripts, leading to miRNA degradation and inhibition of translation [35]. Cell proliferation, colony formation, migration and invasion increase after overexpression of miRNA-21 in breast cancer cells. Studies have shown that miRNA-21 level is a crucial biomarker for breast cancer therapy [35–37]. Due to this fact, we selected the probe DNA and its complementary miRNA-21 sequence.

The oligonucleoties used in the study are listed below:

ssDNA antimiRNA-21 Probe: 5′-TAGCTTATCAGACTGATGTTGA-3′

FAM-miRNA-21 Target: 6-FAM -5′-UAGCUUAUCAGACUGAUGUUGA-3′

*1-Base mismatch sequence (*1-MM*):* 5′-UAGCUUAUAAGACUGAUGUUGA-3′

2.2. Preparation of solutions

The stock synthetic oligonucleotide solutions were dissolved in Tris-EDTA (TE) buffer prepared in-nuclease-free water (10 mM Tris-HCl, pH 8.0, containing 1 mM EDTA) and separated into small 100 μM aliquots. The solutions were stored at −20 °C until use. 20 mM Tris-HCl (pH 7.4) containing 100 mM NaCl and 5 mM MgCl$_2$ prepared with Milli-Q water was used for the FAM-labeled ssDNA immobilization onto micromotors. 20 mM Tris-HCl (pH 7.4) containing 100 mM NaCl and 1 mM EDTA was used for the hybridization procedure. Washing process was performed with 100 μg mL^{-1} of BSA.

2.3. Fabrication of micromotors

W$_5$O$_{14}$ nanowires were synthesized in evacuated and sealed quartz ampoule by a chemical vapor transport reaction (CVT) using iodine as transport agent and nickel as a growth promoter [38]. From WO$_3$ precursor crystals and transport agent, the volatilized WO$_2$I$_2$ molecules were formed and being transported from 1133 to 1009 K under 6.2 °C cm^{-1} temperature gradient. At the colder side, these molecules decomposed to W$_5$O$_{14}$ solid crystals in shape of nanowires and I$_2$ gas. Transport reaction ran for 500 h. The W$_5$O$_{14}$ nanowires of bright blue color and relatively narrow size range were grown around 10 μm in length and 100 nm in diameter.

The uniform polymerization of 3,4-ethylenedioxythiophene (EDOT) on W$_5$O$_{14}$ nanowires was carried out in a capacitive coupled, 13.56 MHz RF rotating plasma reactor as described in our previous reports [39]. Steady-state plasma polymerization conditions were applied for modifications during 30 min and at the working pressure of 6 Pa. To modify the nanowires, EDOT monomer was sent to the rotating chamber and then a 40 Watt of RF rotating plasma power was applied. In Scheme 1, experimental set up and the procedure were summarized. Also, the RF rotating plasma schematic diagram is shown in Fig. S1.

A thin layer of Pt as the catalyst was deposited onto the surfaces of W$_5$O$_{14}$ and W$_5$O$_{14}$/PEDOT microwires by RF magnetron sputtering method: The W$_5$O$_{14}$ and W$_5$O$_{14}$/PEDOT microwires were dispersed in ethanol. This dispersion was drop coated on a glass slide and dried. W$_5$O$_{14}$ and W$_5$O$_{14}$/PEDOT microwires coated glass slides were then coated with Pt layer using RF magnetron sputtering. Sputtering base pressure was 2 mTorr and working pressure was 15 mTorr. Sputtering parameters were 50 Watt, 15 min and Argon gas flow. The distance between Pt target and glass slide substrate was kept at 9 cm for all sputtering processes.

2.4. Characterization

Morphological and elemental properties of W$_5$O$_{14}$/Pt and W$_5$O$_{14}$/PEDOT-Pt micromotors were characterized by electron scanning microscopy (SEM) and energy dispersive X-Ray spectroscopy (EDX) (FEI Quanta FEG 250 Model). X-ray photoelectron spectroscopy (XPS) technique was performed with a Thermo Scientific K-Alpha spectrometer using AlKα radiation as an excitation source at a photo energy of 1486.7 eV. The measurement was carried out using a Kratus AXIS Ultra DLD system under UHV conditions with a base pressure less than 1×10^{-9} mBar. The spectra were acquired with the pass energy of 20 eV and fitted using CasaXPS software. All spectra were calibrated to yield a primary C1s component fitting was applied by Voight functions with 30% Lorentzian component. Optical microscopy videos and images were obtained using a Nikon Eclipse Optic LV100ND microscope with a Nikon digital sight DS-Fi3 camera connected to a computer and operated by Nikon NIS software. Motion videos were recorded at 30 frames per second using a 40× objective. The time interval between two frames is 0.05 s. For each of data points in the speed profile figures, at least 50 measurements were taken into account. To minimize the effect of fuel depletion, only the videos recorded at the first 5 min after fuel addition were taken into account for speed calculation. Free NIS software was used to calculate the speed of micromotors, edit videos and extract pictures.

2.5. Detection of target miRNA-21

W$_5$O$_{14}$/Pt and W$_5$O$_{14}$/PEDOT-Pt micromotors were incubated with 10 μL probe DNA solution (50.0 μM) prepared in 20 mM Tris-HCl (pH 7.4) containing 100 mM NaCl, 5 mM KCl, and 5 mM MgCl$_2$ for different times such as 5, 15, 30 and 60 min with the aim to determine the optimum incubation time. By measuring the speed and fluorescence intensities of the micromotors as depending on incubation time, the optimum incubation time was determined as 30 min for ssDNA probe. The micromotors were washed with 50 μL BSA (washing solution) and centrifuged to remove unbound probe sequences. miRNA-21 detection protocol was depended on the duplex formation (hybridization). The target, 100 nM FAM-labeled miRNA-21 (100 nM, prepared in 20 mM Tris-HCl buffer (pH 7.4) containing 100 mM NaCl, 5 mM KCl and 5 mM MgCl$_2$) was kept in probe DNA immobilized micromotors solution for 15 min of hybridization time. Same procedure was applied for the 1-M sequence. Then, the micromotors were washed with buffer solution. The speed and fluorescence intensities of micromotors were measured using with Nikon Eclipse Ti Optic LV100ND Model microscope (at 520 nm wavelength and fixed frequency, 12 V DIA).

3. Results and discussion

Scanning electron microscopy (SEM) and energy-dispersive X-ray spectroscopy (EDX) experiments were carried out to examine the structural morphology and elemental composition of the W$_5$O$_{14}$/Pt and W$_5$O$_{14}$/PEDOT-Pt micromotors. As seen in Fig. 1, the EDX mapping of micromotors has indicated homogenous distribution of W and Pt components for W$_5$O$_{14}$/Pt micromotors (Fig. 1a) and S, W and Pt components for W$_5$O$_{14}$/PEDOT-Pt micromotors (Fig. 1b). Fig. 1c illustrates the SEM image of ~10 μm-long W$_5$O$_{14}$/Pt
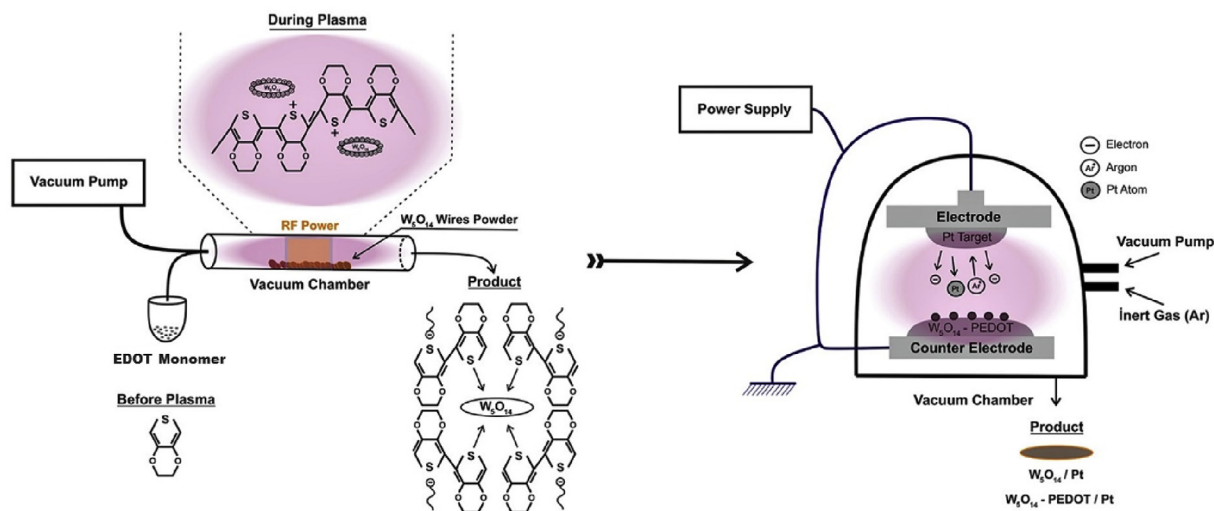
Scheme 1. Schematic diagram representing the micromotor preparation protocol.
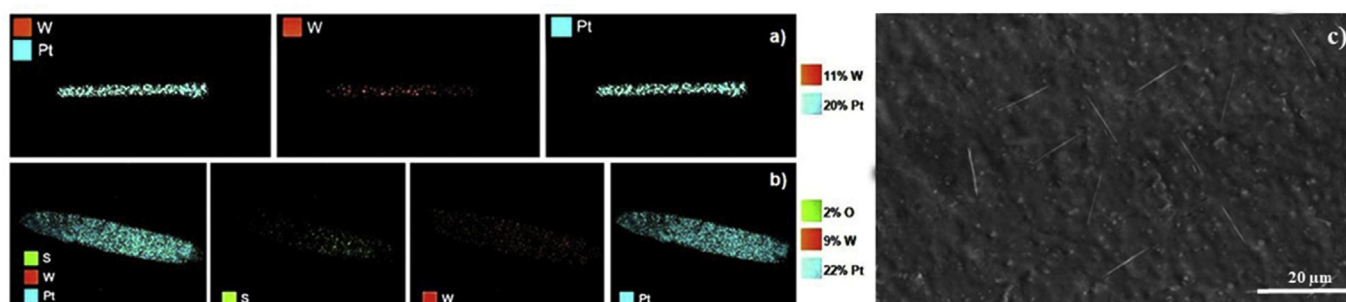
Fig. 1. The EDX analysis results of the a) W_5O_{14}/Pt; b) $W_5O_{14}/PEDOT$-Pt micromotors and c) SEM images of the W_5O_{14}/Pt microwires.

microwires. This figure presented the homogenous and uniform structure of the prepared microwires.

X-ray photoelectron spectroscopy (XPS) of the W_5O_{14}/Pt (Fig. S2) and $W_5O_{14}/PEDOT$-Pt micromotors (Fig. 2) were measured to gain insight into the exact chemical composition of the surface of the microwire motors. XPS spectrum of $W_5O_{14}/PEDOT$-Pt micromotor showed carbon (C1s peak) and sulfur (S2p peak) peaks as different apart from XPS spectrum of W_5O_{14}/Pt micromotor. In Fig. 2a, the W4f, S2p, C1s, Pt4f and O1s peaks appeared at 28.0, 157.0, 283.0, 62.0, and 532.0 eV for $W_5O_{14}/PEDOT$-Pt, respectively. The high resolution XPS spectrum of W_5O_{14}–Pt micromotor exhibited the presence of tungsten (W4f peak), oxygen (O1s) and Platinum (Pt4f peak) (Fig. 2a). The XPS of W4f can well fit with two peaks due to W^{+6} (36.3 eV) and W^{+4} (30.0 eV) (Fig. S2a). The O1s can fit with one peak which is attributed to O–W^{+6} (531.9 eV) (Fig. S2b). The XPS spectrum of Pt4f has two main peaks: the first at 77.1eV and the other one at 73.2 eV refer to Pt ($4f_{5/2}$) and Pt ($4f_{7/2}$), respectively (Fig. S2c) [40]. With the incorporation of PEDOT into the structure, the peaks of W4f$_{7/2}$ were broader and the binding energy region appeared at 30–37 eV (Fig. 2b). After wide peak deconvoluting, two tungsten types were observed as W^{+6} (36.4 eV) [41] and W^{+4} (31.2 eV) [42], respectively. The change of W valence states is attributed to the polymerization. The core level S2p XPS spectra of the synthesized $W_5O_{14}/PEDOT$-Pt can be decomposed into two peaks, at 169.7 and 163.5 eV, that are attributed to the EDOT sulfur atom (Fig. 2c) [43]. In addition, 169.7 in the S2p spectrum corresponds to doped (partially oxidized) sulfur atoms [44]. The core level C1s peak (Fig. 2d) is composed of peak at 285.0 eV

and 288.9 eV, corresponding to C–C/C–H and C=C–O bonds, respectively. Photoelectrons from O1s (Fig. 2e) form peak with the highest point at 531.7 eV, which corresponding to the oxygen bond with O^{-2}-W^{+6} at W_5O_{14} [42]. The spectrum of Pt4f peak (Fig. 2f) can be divided into the two peaks of Pt4f$_{7/2}$ (71.9 eV) and Pt4f$_{5/2}$ (75.0 eV), indicating the presence of metallic Pt (Pt^0) [45,46]. These XPS data confirm the successful formation of the W_5O_{14}/Pt and $W_5O_{14}/PEDOT$-Pt micromotors.

SI Videos 1 and SI Video 2 present the movement of the W_5O_{14}/Pt and $W_5O_{14}/PEDOT$-Pt in a 3% H_2O_2 solution (containing 5% of the Triton X-100 surfactant) during a 3 s period. The W_5O_{14}/Pt and $W_5O_{14}/PEDOT$-Pt micromotors move rapidly in spiral and circular trajectories, with an average speed of 473 μm/s and 342 μm/s, respectively. The micromotor was compared with the previous studies based on conductive polymers and it was found that the speed of the micromotor is higher than PEDOT/Pt–Ni (247 ± 11 μm/s) [47], PAPBA/Ni/Pt (40 μm/s) [48] and PEDOT/Pt (10 μm/s) [49]. Meanwhile, the speed of W_5O_{14}/Pt and $W_5O_{14}/PEDOT$-Pt micromotors were recorded depending on the % H_2O_2 concentration. The velocities of the W_5O_{14}/Pt and $W_5O_{14}/PEDOT$-Pt micromotors increased from 473 μm/s to 545 μm/s and 420 μm/s to 476 μm/s with elevated hydrogen peroxide fuel concentrations from 3% to 10%, respectively. As known from previous works, the speed of catalytic micromotor increases with the increasing concentration of hydrogen peroxide fuel [50]. Also, functionalized-polymer micromotors have played an increasing role as biosensors due to their properties such as biocompatibility, efficient surface area, conductivity, unique chemical and redox properties [51–53]. The speed
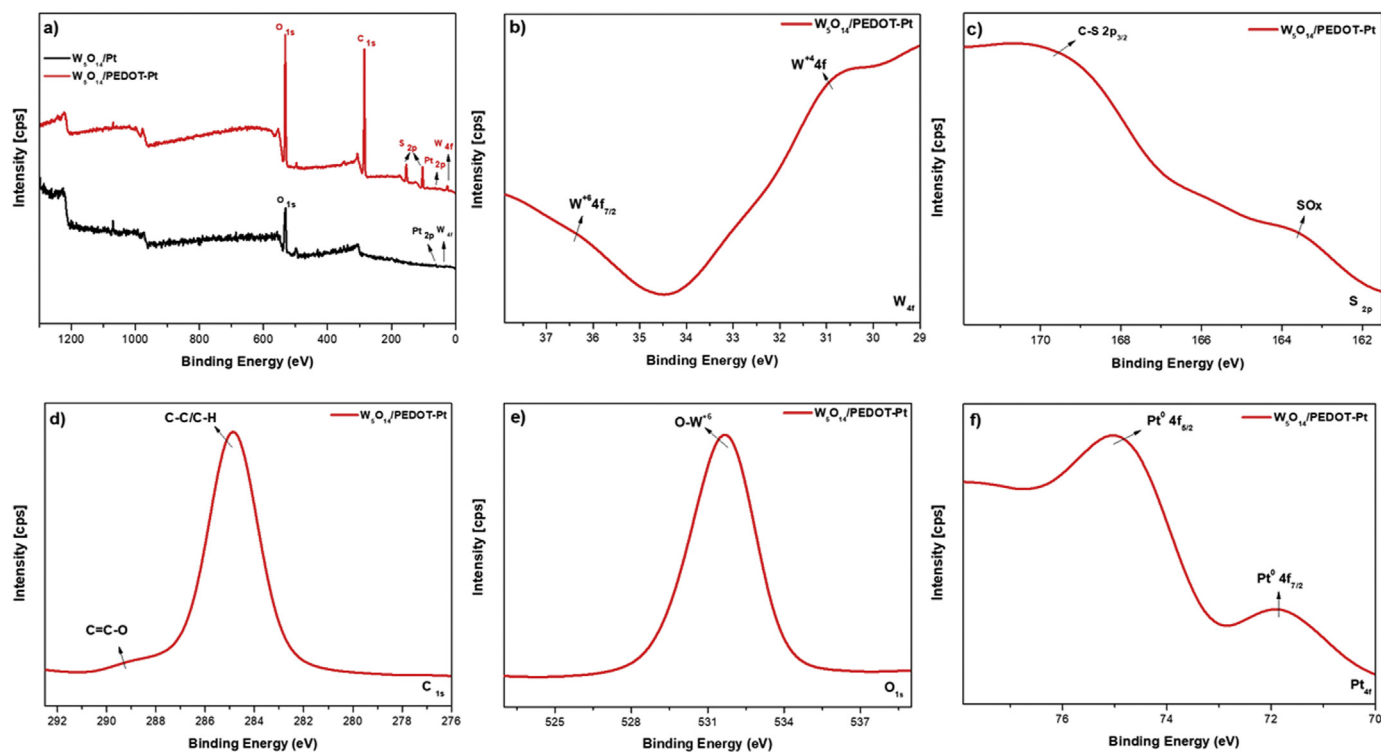
Fig. 2. (a) Broad scan survey spectra of W_5O_{14}/Pt and W_5O_{14}/PEDOT-Pt micromotors and high resolution spectra of (b) W4f, (c) S2p, (d) C1s, (e) O1s, (f) Pt4f of W_5O_{14}/PEDOT-Pt micromotors.

of the W_5O_{14}/PEDOT-Pt micromotors decreased significantly after efficient surface functionalization and the fast original speed of the W_5O_{14}/Pt nanowire motor was also affected by this functionalization [54].

Several crucial optimization parameters, including ssDNA probe-micromotor incubation time, hybridization time between ssDNA probe and FAM-miRNA-21 target that play important roles in the sensing performance were investigated. To evaluate the repeatability of the analytical performances, all tests were repeated three times each. The interaction time of the probe with micromotors was optimized for different times of 5, 15, 30 and 60 min as depending on the change of fluorescence intensity and speed of micromotors (Fig. 3). These studies were carried out with W_5O_{14}/Pt and W_5O_{14}/PEDOT-Pt micromotors. As seen in Fig. 3a–c, there was no significant difference in fluorescence intensities of W_5O_{14}/Pt and W_5O_{14}/PEDOT-Pt micromotors before and after ssDNA probe immobilization since ssDNA probe didn't have any fluorescence property. However, the speed of W_5O_{14}/Pt micromotors decreased from 500 μm/s to 473 μm/s as depending on probe immobilization time for 5 min and 30 min presenting the addition of probe DNA onto the micromotors (Fig. 3b). Also, the speed of W_5O_{14}/PEDOT-Pt micromotors decreased after incubating with the ssDNA probe for different incubation times (Fig. 3d). For 60 min–30 min immobilization times, the speed of the W_5O_{14}/Pt and W_5O_{14}/PEDOT-Pt micromotors remained almost the same. Therefore, the optimum probe incubation time was set at 30 min for the W_5O_{14}/Pt and W_5O_{14}/PEDOT-Pt micromotors.

The hybridization time between the miRNA-21 and the ssDNA probe is another significant parameter that needs to be optimized. Accordingly, to optimize this parameter, various hybridization times, including 5, 15 and 30 min were experimented for 100 nM FAM-labeled miRNA target (Fig. 4). In these studies, both probe DNA immobilized W_5O_{14}/Pt micromotors and W_5O_{14}/PEDOT-Pt

micromotors were used. Since the target was FAM dye labeled, the fluorescence intensities of the micromotors increased significantly (Fig. 4a–c). From the data obtained for the fluorescence intensities, approximately same responses were obtained with 15 min and 30 min of hybridization. Therefore, the results can be concluded as the optimal interaction time is about 15 min where hybridization process occurs effectively in this period. In Fig. 4b–d, the speeds of the micromotors depending on the hybridization times were given. After the hybridization with the target sequence, the speed of micromotors decreased more compared to the ones observed as a result of ssDNA probe immobilization on micromotors. This speed decrease could be associated with complete blocking of the surface by effective formation of ssDNA probe and FAM-labeled miRNA-21 hybrid. The speed of W_5O_{14}/PEDOT-Pt micromotors dramatically decreased from 420 to 78 μm/s after 15 min hybridization time while the speed of the W_5O_{14}/Pt changed only from 473 to 420 μm/s. Plasma coated PEDOT layer increased the effective surface area for ssDNA probe and target interaction facilitating duplex formation on the micromotors.

SI Video 3, 4 and 5 show the trajectories of the probe DNA immobilized W_5O_{14}/Pt micromotors for 5, 15 and 30 hybridization times, respectively. As indicated above, the fluorescent intensities of the W_5O_{14}/Pt based micromotors increase with increasing the hybridization time. On the other hand, SI Video 6, 7 and 8 show the trajectories of the W_5O_{14}/PEDOT-Pt based micromotors for 5, 15 and 30 hybridization times, respectively. In the case of W_5O_{14}/PEDOT-Pt micromotors, the fluorescence intensities increase with increasing the hybridization time similarly to W_5O_{14}/Pt micromotors, while the decrease in the speed of the micromotors is much more as given in Fig. 4. The reason of this decrease in the speed of the micromotors is the hybridization that occurred on the outer surface of the ssDNA probe functionalized micromotors [54]. In addition, probe DNA could bound on the surface of W_5O_{14} through the hydrophobic
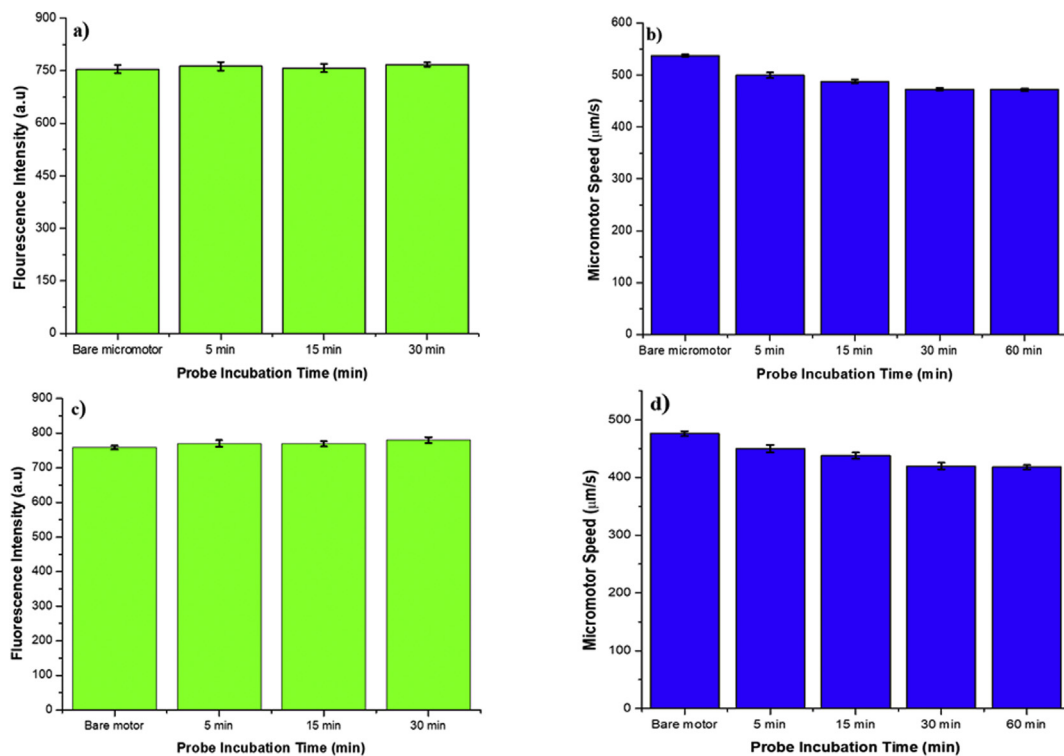
Fig. 3. ssDNA probe immobilization onto W_5O_{14}/Pt and W_5O_{14}/PEDOT-Pt micromotors: (a–c) fluorescence intensities and (c–d) speed of micromotors with respect to increasing incubation time (n = 3).
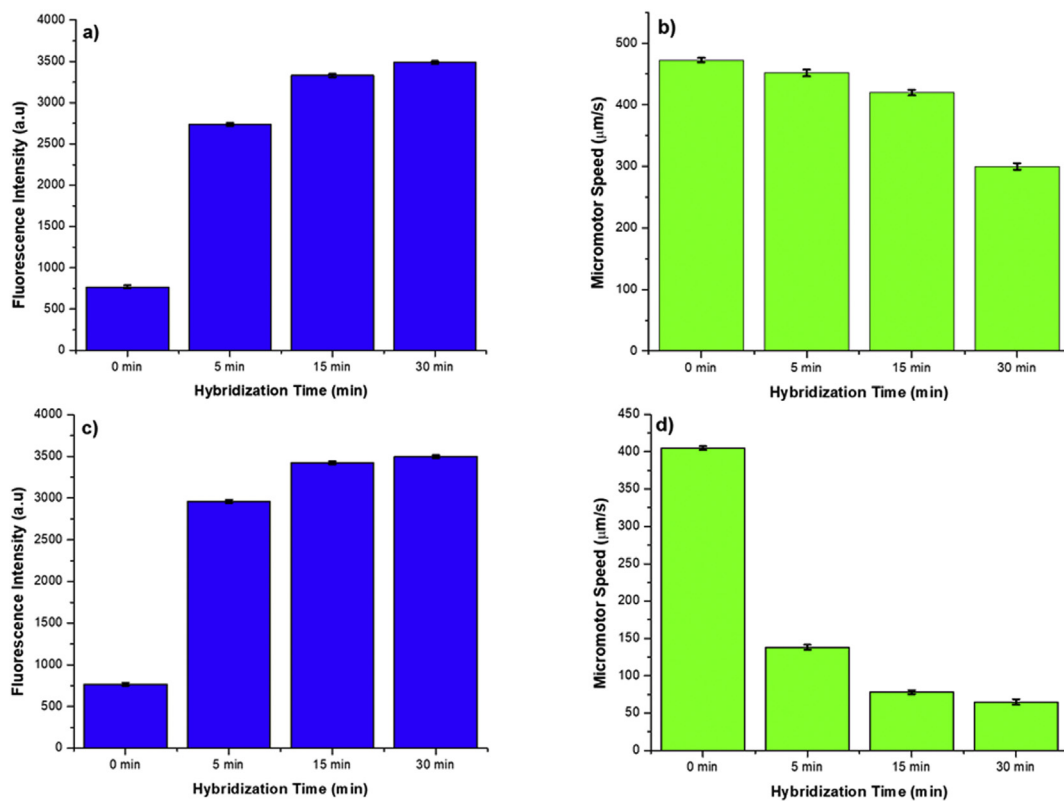
Fig. 4. The effects of hybridization time on fluorescence intensity and micromotor speed for W_5O_{14}/Pt (a–b) and W_5O_{14}/PEDOT-Pt (c–d), respectively (n = 3).

interaction via van der Waals forces between the nucleobases of ssDNA probe, while the sugars in the ssDNA backbone created strong electrostatic interaction [37,54,55]. Plasma PEDOT modification of W_5O_{14} created more effective surfaces for probe DNA immobilization. W_5O_{14}/PEDOT-Pt micromotors had the electrostatic interactions between negatively charged phosphate groups of ssDNA probe and the positively charged conductive polymer, also hydrogen bonding interactions in parallel to the literature [56,57].

To demonstrate the applicability of the micromotors approach towards the miRNA-21 detection, the fluorescence signals and micromotor speeds were examined after incubating various concentrations of FAM-miRNA-21 target with ssDNA probe immobilized W_5O_{14}/Pt and W_5O_{14}/PEDOT-Pt micromotors for 15 min hybridization time. A substantial increase in the fluorescence intensity was noticed after the hybridization occurred on the micromotor surfaces. Our data showed good correlation between the change in fluorescence intensity and speed of micromotor and the miRNA-21 concentration (Fig. 5a—d). As seen from the calibration curves in Fig. 5a, linearity was observed between increasing target concentration (1 nM—100 nM) and fluorescence intensity (2096 a.u to 3330 a.u) of the probe DNA immobilized W_5O_{14}/Pt micromotors. Same tendencies were observed when the changes in the speeds were evaluated. In Fig. 5b, the changes in these micromotor speeds decreased from 380 μm/s to 120 μm/s depending on the increasing target concentration from 0.1 to 100 nM. Also, the inset bar figures show the fluorescence intensity based on target concentration. The fluorescence intensities of probe DNA immobilized W_5O_{14}/PEDOT-Pt micromotors increased from 2076 a.u. (0.1 nM) to 3425 a.u. (100 nM) (Fig. 5c) (n = 3). As the target concentration increased from 0.1 nM to 100 nM, the speeds of

micromotors decreased from 250 μm/s to 78 μm/s for W_5O_{14}/PEDOT-Pt micromotors (Fig. 5d).

The speed of the micromotors firstly decreased after ssDNA immobilization as given above. This speed was still sufficient to use these micromotors in the detection of target miRNA-21. In the presence of miRNA-21, the micromotor speed further reduced after hybridization. The decreased speed may be associated with partial blocking by hybridized FAM-labeled miRNA-21 and poising some catalytic side of Pt by sulfur atoms for W_5O_{14}/PEDOT-Pt micromotors [55—58,58—61]. The decrease in speed of probe ssDNA immobilized micromotors was proportional to the analyte miRNA-21 concentration. These results along with the fluorescence intensity illustrated that the developed micromotors had the capability of detecting miRNA-21 as a cancer biomarker.

Based on the changes in the fluorescence intensities, the limit of detection (LOD) values were calculated from calibration graphs for both micromotors. A commonly used definition for the limit of detection was used as the blank signal plus three standard deviations of the blank [59].

They were found as 0.18 nM for the probe DNA immobilized W_5O_{14}/Pt micromotors and 0.028 nM for the probe DNA immobilized W_5O_{14}/PEDOT-Pt micromotors (n = 3). Another calculation could also be done for these microstructures since they had a very good correlation in terms of movement depending on the target concentrations. In this context, based on the changes in the speeds of micromotors, LOD values were found as 0.11 nM and 0.021 nM for these micromotors, respectively (n = 3). Polymer modification increased the analytical performance of the micromotors in terms of higher sensitivity resulting lower LOD values [60]. Incorporation of polymer into the micromotors could affect the effective surface
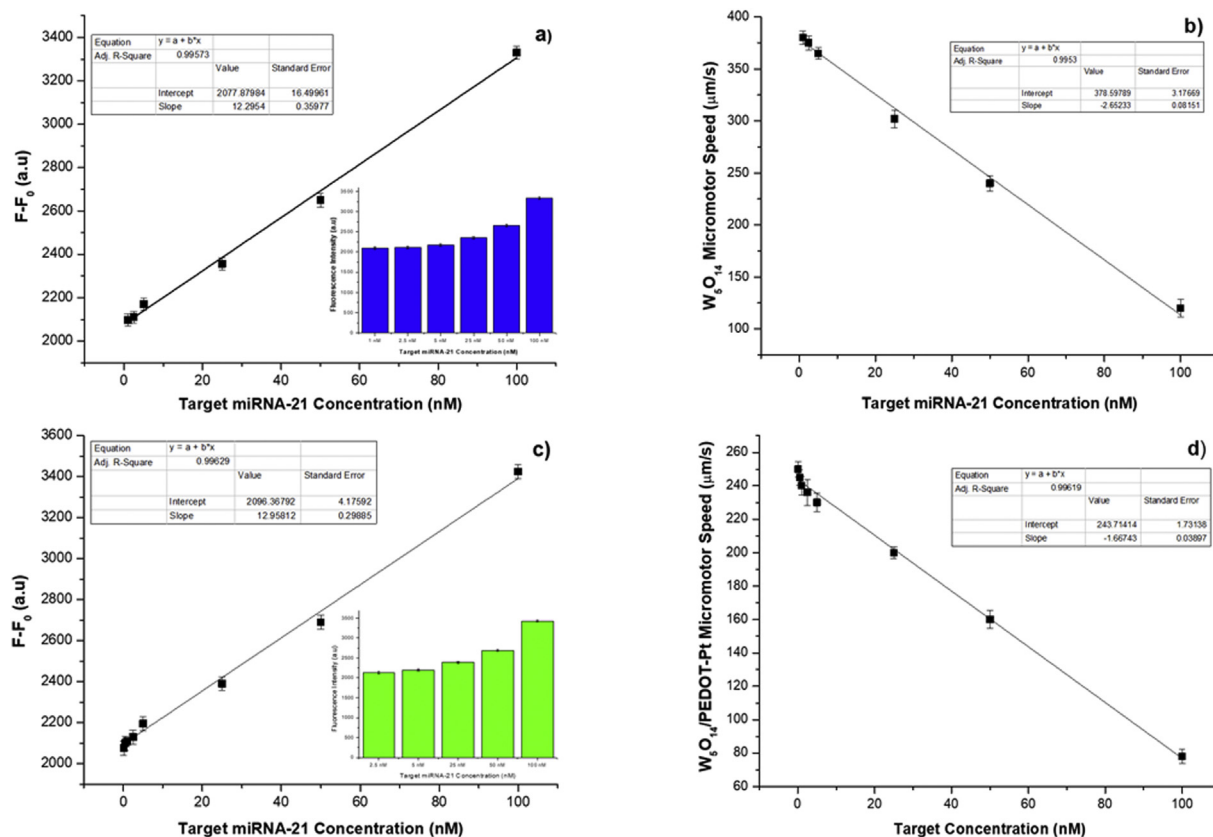
Fig. 5. Calibration curves based on fluorescence intensities and inset; bar graphs (a—c) and speeds (b—d) of W_5O_{14}/Pt (a,b) and W_5O_{14}/PEDOT-Pt (c,d) micromotors based on target concentration (0.1 nM, 0.5 nM, 1 nM, 2.5 nM, 5 nM, 25 nM, 50 nM, 100 nM, respectively) (n = 3, 15 min of hybridization).

Table 1
Comparison of the detection performances of different nano/micromaterials for miRNA-21 detection.

Method of Detection	Nano/Micromaterials	Detection Limit	Reference
Fluorescence	Gold-nanorod functionalized polydiacetylene microtube	1.0×10^{-11} mol L^{-1}	[62]
Fluorescence	Gold nanoparticle	9.0×10^{-15} mol L^{-1}	[63]
Fluorescence	MnO_2 nanosheets	3.3×10^{-10} mol L^{-1}	[64]
Colorimetric	Graphene/gold-nanoparticle	3.2×10^{-9} mol L^{-1}	[65]
Fluorescence	Graphene oxide	1.60×10^{-13} mol L^{-1}	[66]
Fluorescence	Reduced graphene oxide/Ni–Pt microtube	1.3×10^{-6} mol L^{-1}	[68]
Fluorescence	W_5O_{14}/PEDOT-Pt	2.8×10^{-11} mol L^{-1}	This study
Fluorescence	W_5O_{14}–Pt	1.8×10^{-10} mol L^{-1}	This study
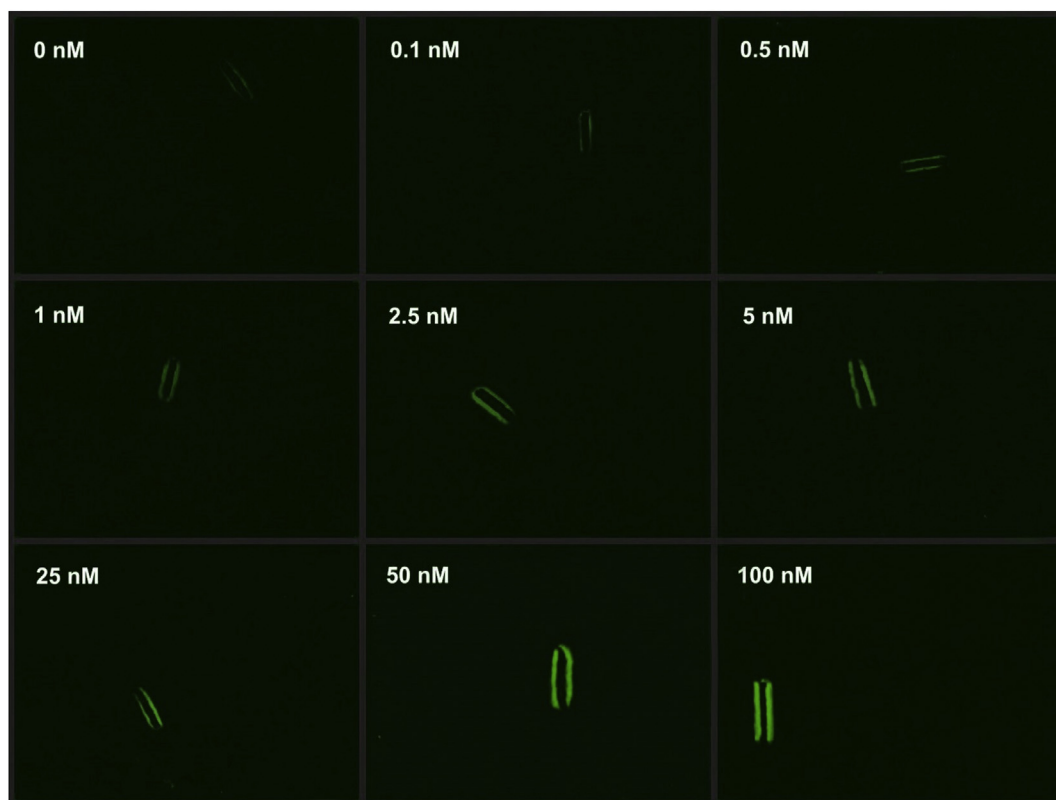
Fig. 6. Fluorescence-based optical microscope images of the probe DNA immobilized W_5O_{14}/PEDOT-Pt micromotors for different target concentrations (15 min of incubation).

area for ssDNA probe immobilization and thus yielding higher fluorescence intensities after hybridization [61]. There was a slight increase in the fluorescence intensity of the W_5O_{14}/PEDOT-Pt micromotor. Meanwhile, with the existence of PEDOT into the structure, a sharp decrease occurred in the speed of the micromotor as seen in Fig. 5 presenting the use of biosensor also based on micromotor speed changes. Furthermore, with the entrance of the polymer into the structure according to the calculated LOD values, the LOD of the probe DNA immobilized W_5O_{14}/PEDOT-Pt micromotor is approximately 10 times higher than probe DNA immobilized W_5O_{14}/Pt micromotor. Thus, the findings offered promising results for early cancer diagnosis and clinical applications. The sensor performances of the synthesized microstructures were compared to the existing biosensors in the literature used for the detection of miRNA-21 (Table 1) [62–66]. It can be concluded that the both biosensing platforms prepared in the work have comparable results with the previous studies. The values based on the fluorescence intensities were placed into Table 1 and the approach in fluorescence intensity increments due to the FAM-labeled target was used. FAM dye has fluorescence signal at λ_{em} 520 nm [67].

Related optical microscope images of the probe DNA immobilized W_5O_{14}/PEDOT-Pt micromotors for different target concentrations are given in Fig. 6. Fluorescence intensity increments onto micromotors can be clearly seen from these optical images. At 100 nM target concentration, there is a full surface coverage with a high fluorescence intensity.

Furthermore, experiments performed with the single-base mismatch (1-MM) exhibited that probe DNA immobilized W_5O_{14}/Pt and W_5O_{14}/PEDOT-Pt micromotors were able to differentiate miRNA-21 target and 1-MM successfully. Fig. 7 presents the comparison of the fluorescence intensities of the micromotors after the incubation of target (100 nM) and 1-MM (100 nM) sequences for 15 min of incubation. These results showed that the probe immobilized W_5O_{14}/Pt and W_5O_{14}/PEDOT-Pt micromotors are quite selective for miRNA-21 target sequence.

4. Conclusions

In conclusion, synthesis, characterization and bioapplications of W_5O_{14}/Pt and W_5O_{14}/PEDOT-Pt micromotors were performed for
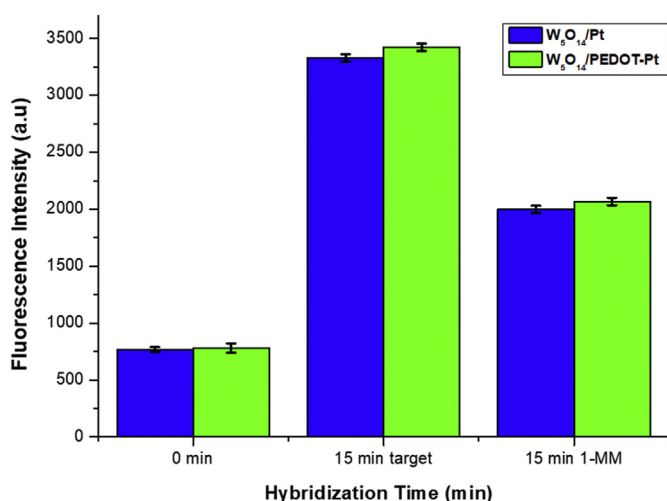
Fig. 7. The effects of target and 1-MM on fluorescence intensities for DNA probe immobilized W_5O_{14}/Pt and W_5O_{14}/PEDOT-Pt micromotors (n = 3, target and 1-MM concentration: 100 nM).

the first time in this paper. The critical comparison of the polymer modified structure to the unmodified form was made and the differences for miRNA-21 detection were considered. RF rotating plasma modification was shown to be particularly very novel for preparing such polymer-based catalytic micromotors. The plasma polymerization process had the advantage of rapid and homogeneous deposition of thin polymer layers onto the nanowires. Dual response of the probe DNA immobilized micromotors based on the fluorescence intensities and micromotor speeds were considered as the indicators of hybridization. The remarkable speed of the new micromotors reflected in their high ability for biomarker responsive performance. Especially, probe DNA immobilized polymer modified W_5O_{14}/Pt micromotor presented a wide linear target concentration range of 0.1 and 100 nM with a detection limit of 0.028 nM (n = 3). Thus, polymer modification improved the analytical performance of the micromotors presenting effective and active surface areas for probe immobilization and hybridization. The probe DNA immobilized W_5O_{14}/PEDOT-Pt micromotor had good sensitivity for the miRNA-21 target detection. These kind of wire catalytic micromotors are expected to be of importance for highly sensitive and selective detection of miRNA-21 in early diagnosis of cancer.

CRediT authorship contribution statement

Gamze Celik Cogal: Writing - original draft. **Gozde Yurdabak Karaca:** Investigation, Writing - review & editing. **Emre Uygun:** Software, Validation. **Filiz Kuralay:** Conceptualization, Methodology, Writing - review & editing. **Lutfi Oksuz:** Funding acquisition. **Maja Remskar:** Methodology. **Aysegul Uygun Oksuz:** Writing - original draft, Supervision.

Declaration of competing interest

The authors declare that they have no known competing financial interests or personal relationships that could have appeared to influence the work reported in this paper.

Acknowledgements

Appendix A. Supplementary data

Supplementary data to this article can be found online at https://doi.org/10.1016/j.aca.2020.07.010.

References

[1] A. Barreiro, R. Rurali, E.R. Hernández, J. Moser, T. Pichler, L. Forró, A. Bachtold, Subnanometer motion of cargoes driven by thermal gradients along carbon nanotubes, Science 320 (80) (2008) 775–778, https://doi.org/10.1126/science.1155559.

[2] X. Lin, Z. Wu, Y. Wu, M. Xuan, Q. He, Self-propelled micro-/nanomotors based on controlled assembled architectures, Adv. Mater. 28 (2016) 1060–1072, https://doi.org/10.1002/adma.201502583.

[3] L. Qin, M.J. Banholzer, X. Xu, L. Huang, C.A. Mirkin, Rational design and synthesis of catalytically driven nanorotors, J. Am. Chem. Soc. 129 (2007) 14870–14871, https://doi.org/10.1021/ja0772391.

[4] R.F. Ismagilov, A. Schwartz, N. Bowden, G.M. Whitesides, Autonomous movement and self-assembly, Angew. Chem. 114 (2002) 674–676, https://doi.org/10.1002/1521-3757(20020215)114:4<674::aid-ange674>3.0.co;2-z.

[5] J. Wu, S. Balasubramanian, D. Kagan, K.M. Manesh, S. Campuzano, J. Wang, Motion-based DNA detection using catalytic nanomotors, Nat. Commun. 1 (2010) 1–6, https://doi.org/10.1038/ncomms1035.

[6] W.F. Paxton, K.C. Kistler, C.C. Olmeda, A. Sen, S.K. St Angelo, Y. Cao, T.E. Mallouk, P.E. Lammert, V.H. Crespi, Catalytic nanomotors: autonomous movement of striped nanorods, J. Am. Chem. Soc. 126 (2004) 13424–13431, https://doi.org/10.1021/ja047697z.

[7] S. Sundararajan, P.E. Lammert, A.W. Zudans, V.H. Crespi, A. Sen, Catalytic motors for transport of colloidal cargo, Nano Lett. 8 (2008) 1271–1276, https://doi.org/10.1021/nl072275j.

[8] D. Kagan, P. Calvo-Marzal, S. Balasubramanian, S. Sattayasamitsathit, K.M. Manesh, G.U. Flechsig, J. Wang, Chemical sensing based on catalytic nanomotors: motion-based detection of trace silver, J. Am. Chem. Soc. 131 (2009) 12082–12083, https://doi.org/10.1021/ja905142q.

[9] Y. Wang, S.T. Fei, Y.M. Byun, P.E. Lammert, V.H. Crespi, A. Sen, T.E. Mallouk, Dynamic interactions between fast microscale rotors, J. Am. Chem. Soc. 131 (2009) 9926–9927, https://doi.org/10.1021/ja904827j.

[10] W. Wang, T.Y. Chiang, D. Velegol, T.E. Mallouk, Understanding the efficiency of autonomous nano- and microscale motors, J. Am. Chem. Soc. 135 (2013) 10557–10565, https://doi.org/10.1021/ja405135f.

[11] B. Kovalerchuk, J. Schwing, Visual and spatial analysis. Advances in data mining, reasoning, and problem solving, Library 6 (2004) 576, https://doi.org/10.1039/c3ib40165k.NANOPARTICLES.

[12] M. Guix, A.K. Meyer, B. Koch, O.G. Schmidt, Carbonate-based Janus micromotors moving in ultra-light acidic environment generated by HeLa cells in situ, Sci. Rep. 6 (2016) 1–7, https://doi.org/10.1038/srep21701.

[13] D.J. Bharali, S.A. Mousa, Emerging nanomedicines for early cancer detection and improved treatment: current perspective and future promise, Pharmacol. Ther. 128 (2010) 324–335, https://doi.org/10.1016/j.pharmthera.2010.07.007.

[14] A. Kozomara, S. Griffiths-Jones, MiRBase: integrating microRNA annotation and deep-sequencing data, Nucleic Acids Res. 39 (2011) 152–157, https://doi.org/10.1093/nar/gkq1027.

[15] A. Kozomara, S. Griffiths-Jones, MiRBase: annotating high confidence microRNAs using deep sequencing data, Nucleic Acids Res. 42 (2014) 68–73, https://doi.org/10.1093/nar/gkt1181.

[16] J. Li, D. Li, R. Yuan, Y. Xiang, Biodegradable MnO2 nanosheet-mediated signal amplification in living cells enables sensitive detection of down-regulated intracellular MicroRNA, ACS Appl. Mater. Interfaces 9 (2017) 5717–5724, https://doi.org/10.1021/acsami.6b13073.

[17] S. Campuzano, R.M. Torrente-Rodríguez, E. López-Hernández, F. Conzuelo, R. Granados, J.M. Sánchez-Puelles, J.M. Pingarrón, Magnetobiosensors based on viral protein p19 for microrna determination in cancer cells and tissues, Angew. Chem. Int. Ed. 53 (2014) 6168–6171, https://doi.org/10.1002/anie.201403270.

[18] T. Kilic, S.N. Topkaya, D. Ozkan Ariksoysal, M. Ozsoz, P. Ballar, Y. Erac, O. Gozen, Electrochemical based detection of microRNA, mir21 in breast cancer cells, Biosens, Bioelectron 38 (2012) 195–201, https://doi.org/10.1016/j.bios.2012.05.031.

[19] A.M. Ardekani, M.M. Naeini, The role of microRNAs in human diseases, Avicenna J. Med. Biotechnol. (AJMB) 2 (2010) 161–179.

[20] B. Esteban-Fernández De Ávila, A. Martín, F. Soto, M.A. Lopez-Ramirez, S. Campuzano, G.M. Vásquez-Machado, W. Gao, L. Zhang, J. Wang, Single cell real-time miRNAs sensing based on nanomotors, ACS Nano 9 (2015) 6756–6764, https://doi.org/10.1021/acsnano.5b02807.

[21] J.C. Hill, K.S. Choi, Effect of electrolytes on the selectivity and stability of n-type WO 3 photoelectrodes for use in solar water oxidation, J. Phys. Chem. C 116 (2012) 7612–7620, https://doi.org/10.1021/jp209909b.

[22] P.R. Solanki, A. Kaushik, V.V. Agrawal, B.D. Malhotra, Nanostructured metal oxide-based biosensors, NPG Asia Mater. 3 (2011) 17–24, https://doi.org/10.1038/asiamat.2010.137.

[23] D. Sandil, S. Kumar, K. Arora, S. Srivastava, B.D. Malhotra, S.C. Sharma, N.K. Puri, Biofunctionalized nanostructured tungsten trioxide based sensor for cardiac biomarker detection, Mater. Lett. 186 (2017) 202–205, https://doi.org/

10.1016/j.matlet.2016.09.107.

[24] H.L. Shuai, K.J. Huang, L.L. Xing, Y.X. Chen, Ultrasensitive electrochemical sensing platform for microRNA based on tungsten oxide-graphene composites coupling with catalyzed hairpin assembly target recycling and enzyme signal amplification, Biosens. Bioelectron. 86 (2016) 337–345, https://doi.org/10.1016/j.bios.2016.06.057.

[25] C.Y. Su, H.C. Lin, T.K. Yang, C.K. Lin, Structure and optical properties of tungsten oxide nanomaterials prepared by a modified plasma arc gas condensation technique, J. Nanoparticle Res. 12 (2010) 1755–1763, https://doi.org/10.1007/s11051-009-9730-y.

[26] T. Darmanin, F. Guittard, Superhydrophobic fiber mats by electrodeposition of fluorinated poly(3,4-ethyleneoxythiathiophene), J. Am. Chem. Soc. 133 (2011) 15627–15634, https://doi.org/10.1021/ja205283b.

[27] Y.-Z. Long, M.-M. Li, C. Gu, M. Wan, J.-L. Duvail, Z. Liu, Z. Fan, Recent advances in synthesis, physical properties and applications of conducting polymer nanotubes and nanofibers, Prog. Polym. Sci. 36 (2011) 1415–1442, https://doi.org/10.1016/j.progpolymsci.2011.04.001.

[28] S.C. Luo, E.M. Ali, N.C. Tansil, H.H. Yu, S. Gao, E.A.B. Kantchev, J.Y. Ying, Poly(3,4-ethylenedioxythiophene) (PEDOT) nanobiointerfaces: thin, ultra-smooth, and functionalized PEDOT films with in vitro and in vivo biocompatibility, Langmuir 24 (2008) 8071–8077, https://doi.org/10.1021/la800333g.

[29] J. Sekine, S.C. Luo, S. Wang, B. Zhu, H.R. Tseng, H.H. Yu, Functionalized conducting polymer nanodots for enhanced cell capturing: the synergistic effect of capture agents and nanostructures, Adv. Mater. 23 (2011) 4788–4792, https://doi.org/10.1002/adma.201102151.

[30] G. Wallace, G. Spinks, Conducting polymers - bridging the bionic interface, Soft Matter 3 (2007) 665–671, https://doi.org/10.1039/b618204f.

[31] S.C. Luo, H. Xie, N. Chen, H.H. Yu, Trinity DNA detection platform by ultra-smooth and functionalized pedot biointerfaces, ACS Appl. Mater. Interfaces 1 (2009) 1414–1419, https://doi.org/10.1021/am900117e.

[32] L. Xia, Z. Wei, M. Wan, Conducting polymer nanostructures and their application in biosensors, J. Colloid Interface Sci. 341 (2010) 1–11, https://doi.org/10.1016/j.jcis.2009.09.029.

[33] A. Chalupniak, E. Morales-Narvaez, A. Merkoçi, Micro and nanomotors in diagnostics, Adv. Drug Deliv. Rev. 95 (2015) 104–116, https://doi.org/10.1016/j.addr.2015.09.004.

[34] M. Guix, C.C. Mayorga-martinez, A. Merkoc, Nano/micromotors in (bio) chemical science applications, Chem. Rev. (2014) 2646–2649, https://doi.org/10.1021/cr400273r.

[35] C. Zhang, K. Liu, T. Li, J. Fang, Y. Ding, L. Sun, T. Tu, X. Jiang, S. Du, J. Hu, W. Zhu, H. Chen, X. Sun, MiR-21: a gene of dual regulation in breast cancer, Int. J. Oncol. 48 (2016) 161–172, https://doi.org/10.3892/ijo.2015.3232.

[36] X. Qiu, J. Xu, J. Guo, A. Yahia-Ammar, N.I. Kapetanakis, I. Duroux-Richard, J.J. Unterluggauer, N. Golob-Schwarzl, C. Regeard, C. Uzan, S. Gouy, M. Dubow, J. Haybaeck, F. Apparailly, P. Busson, N. Hildebrandt, Advanced microRNA-based cancer diagnostics using amplified time-gated FRET, Chem. Sci. 9 (2018) 8046–8055, https://doi.org/10.1039/c8sc03121e.

[37] H. Wang, Z. Tan, H. Hu, H. Liu, T. Wu, C. Zheng, X. Wang, Z. Luo, J. Wang, S. Liu, Z. Lu, J. Tu, MicroRNA-21 promotes breast cancer proliferation and metastasis by targeting LZTFL1, BMC Canc. 19 (2019) 1–13, https://doi.org/10.1186/s12885-019-5951-3.

[38] M. Remškar, J. Kovac, M. Viršek, M. Mrak, A. Jesih, A. Seabaugh, W5O14 nanowires, Adv. Funct. Mater. 17 (2007) 1974–1978, https://doi.org/10.1002/adfm.200601150.

[39] S.E. Ela, M. Remskar, G.Y. Karaca, L. Oksuz, E. Uygun, A.U. Oksuz, RF plasma modified W5O14 and MoS2 hybrid nanostructures and photovoltaic properties, Part, Sci. Technol. 37 (2019) 612–618, https://doi.org/10.1080/02726351.2017.1414091.

[40] X. Ji, K.T. Lee, R. Holden, L. Zhang, J. Zhang, G.A. Botton, M. Couillard, L.F. Nazar, Nanocrystalline intermetallics on mesoporous carbon for direct formic acid fuel cell anodes, Nat. Chem. 2 (2010) 286–293, https://doi.org/10.1038/nchem.553.

[41] G. Wang, Y. Ling, H. Wang, X. Yang, C. Wang, J.Z. Zhang, Y. Li, Hydrogen-treated WO 3 nanoflakes show enhanced photostability, Energy Environ. Sci. 5 (2012) 6180–6187, https://doi.org/10.1039/c2ee03158b.

[42] M. Katoh, Y. Takeda, Chemical state analysis of tungsten and tungsten oxides using an electron probe microanalyzer, Japanese J. Appl. Physics, Part 1 Regul. Pap. Short Notes Rev. Pap. 43 (2004) 7292–7293, https://doi.org/10.1143/JJAP.43.7292.

[43] V. Callegari, L. Gence, S. Melinte, S. Demoustier-Champagne, Electrochemically template-grown multi-segmented gold-conducting polymer nanowires with tunable electronic behavior, Chem. Mater. 21 (2009) 4241–4247, https://doi.org/10.1021/cm901224u.

[44] H. Zhao, L. Liu, Y. Fang, R. Vellacheri, Y. Lei, Nickel nanopore arrays as promising current collectors for constructing solid-state supercapacitors with ultrahigh rate performance, Front. Chem. Sci. Eng. 12 (2018) 339–345, https://doi.org/10.1007/s11705-018-1699-6.

[45] Y. Hang Li, J. Xing, Z. Jia Chen, Z. Li, F. Tian, L. Rong Zheng, H. Feng Wang, P. Hu, H. Jun Zhao, H. Gui Yang, Unidirectional suppression of hydrogen oxidation on oxidized platinum clusters, Nat. Commun. 4 (2013) 1–7, https://doi.org/10.1038/ncomms3500.

[46] S.J. Wang, H.H. Park, Properties of one-step synthesized Pt nanoparticle-doped poly(3,4-ethylenedioxy thiophen):poly(styrenesulfonate) hybrid films, Thin

Solid Films 518 (2010) 7185–7190, https://doi.org/10.1016/j.tsf.2010.04.084.

[47] J. Orozco, A. Cortés, G. Cheng, S. Sattayasamitsathit, W. Gao, X. Feng, Y. Shen, J. Wang, Molecularly imprinted polymer-based catalytic micromotors for selective protein transport, J. Am. Chem. Soc. 135 (2013) 5336–5339, https://doi.org/10.1021/ja4018545.

[48] F. Kuralay, S. Sattayasamitsathit, W. Gao, A. Uygun, A. Katzenberg, J. Wang, Self-propelled carbohydrate-sensitive microtransporters with built-in boronic acid recognition for isolating sugars and cells, J. Am. Chem. Soc. 134 (2012) 15217–15220, https://doi.org/10.1021/ja306080t.

[49] W. Gao, S. Sattayasamitsathit, A. Uygun, A. Pei, A. Ponedal, J. Wang, Polymer-based tubular microbots: role of composition and preparation, Nanoscale 4 (2012) 2447–2453, https://doi.org/10.1039/c2nr30138e.

[50] W. Gao, S. Sattayasamitsathit, J. Orozco, J. Wang, Highly efficient catalytic microengines: template electrosynthesis of polyaniline/platinum microtubes, J. Am. Chem. Soc. 133 (2011) 11862–11864, https://doi.org/10.1021/ja203773g.

[51] T. Darmanin, F. Guittard, Superhydrophobic fiber mats by electrodeposition of fluorinated poly(3,4-ethyleneoxythiathiophene), J. Am. Chem. Soc. 133 (2011) 15627–15634, https://doi.org/10.1021/ja205283b.

[52] Y.Z. Long, M.M. Li, C. Gu, M. Wan, J.L. Duvail, Z. Liu, Z. Fan, Recent advances in synthesis, physical properties and applications of conducting polymer nanotubes and nanofibers, Prog. Polym. Sci. 36 (2011) 1415–1442, https://doi.org/10.1016/j.progpolymsci.2011.04.001.

[53] J. Sekine, S.C. Luo, S. Wang, B. Zhu, H.R. Tseng, H.H. Yu, Functionalized conducting polymer nanodots for enhanced cell capturing: the synergistic effect of capture agents and nanostructures, Adv. Mater. 23 (2011) 4788–4792, https://doi.org/10.1002/adma.201102151.

[54] M. García, J. Orozco, M. Guix, W. Gao, S. Sattayasamitsathit, A. Escarpa, A. Merkoçi, J. Wang, Micromotor-based lab-on-chip immunoassays, Nanoscale 5 (2013) 1325–1331, https://doi.org/10.1039/C2NR32400H.

[55] S. Balasubramanian, D. Kagan, C.M. Jack Hu, S. Campuzano, M.J. Lobo-Castañon, N. Lim, D.Y. Kang, M. Zimmerman, L. Zhang, J. Wang, Micromachine-enabled capture and isolation of cancer cells in complex media, Angew. Chem. Int. Ed. 50 (2011) 4161–4164, https://doi.org/10.1002/anie.201100115.

[56] M.S. Draz, K.M. Kochehbyoki, A. Vasan, D. Battalapalli, A. Sreeram, M.K. Kanakasabapathy, S. Kallakuri, A. Tsibris, D.R. Kuritzkes, H. Shafiee, DNA engineered micromotors powered by metal nanoparticles for motion based cellphone diagnostics, Nat. Commun. 9 (2018), https://doi.org/10.1038/s41467-018-06727-8.

[57] K. Van Nguyen, S.D. Minteer, DNA-functionalized Pt nanoparticles as catalysts for chemically powered micromotors: toward signal-on motion-based DNA biosensor, Chem. Commun. 51 (2015) 4782–4784, https://doi.org/10.1039/c4cc10250a.

[58] T. Xu, W. Gao, L.P. Xu, X. Zhang, S. Wang, Fuel-free synthetic micro-/nano-machines, Adv. Mater. 29 (2017), https://doi.org/10.1002/adma.201603250.

[59] U.K. Parashar, N.R. Nirala, C. Upadhyay, P.S. Saxena, A. Srivastava, Urease immobilized fluorescent gold nanoparticles for urea sensing, Appl. Biochem. Biotechnol. 176 (2015) 480–492, https://doi.org/10.1007/s12010-015-1589-z.

[60] B. Jurado-Sánchez, A. Escarpa, J. Wang, Lighting up micromotors with quantum dots for smart chemical sensing, Chem. Commun. 51 (2015) 14088–14091, https://doi.org/10.1039/c5cc04726a.

[61] Á. Molinero Fernández, M. Moreno-Guzmán, L. Arruza, M.Á. López, A. Escarpa, Polymer-based micromotors fluorescence immunoassay for on the move sensitive procalcitonin determination in very low birth weight infants' plasma, ACS Sens. (2020), https://doi.org/10.1021/acssensors.9b02515.

[62] Y. Zhu, D. Qiu, G. Yang, M. Wang, Q. Zhang, P. Wang, H. Ming, D. Zhang, Y. Yu, G. Zou, R. Badugu, J.R. Lakowicz, Selective and sensitive detection of MiRNA-21 based on gold-nanorod functionalized polydiacetylene microtube waveguide, Biosens. Bioelectron. 85 (2016) 198–204, https://doi.org/10.1016/j.bios.2016.05.019.

[63] T. Wei, D. Du, Z. Wang, W. Zhang, Y. Lin, Z. Dai, Rapid and sensitive detection of microRNA via the capture of fluorescent dyes-loaded albumin nanoparticles around functionalized magnetic beads, Biosens. Bioelectron. 94 (2017) 56–62, https://doi.org/10.1016/j.bios.2017.02.044.

[64] W. Ouyang, Z.H. Liu, G.F. Zhang, Z. Chen, L. Guo, Z. Lin, B. Qiu, G. Chen, Enzyme-free fluorescent biosensor for miRNA-21 detection based on MnO2 nanosheets and catalytic hairpin assembly amplification, Anal. Methods. 8 (2016) 8492–8497, https://doi.org/10.1039/c6ay02551j.

[65] H. Zhao, Y. Qu, F. Yuan, X. Quan, A visible and label-free colorimetric sensor for miRNA-21 detection based on peroxidase-like activity of graphene/gold-nanoparticle hybrids, Anal. Methods. 8 (2016) 2005–2012, https://doi.org/10.1039/c5ay03296b.

[66] S. Guo, F. Yang, Y. Zhang, Y. Ning, Q. Yao, G.J. Zhang, Amplified fluorescence sensing of miRNA by combination of graphene oxide with duplex-specific nuclease, Anal. Methods. 6 (2014) 3598–3603, https://doi.org/10.1039/c4ay00345d.

[67] C.H. Lu, H.H. Yang, C.L. Zhu, X. Chen, G.N. Chen, A graphene platform for sensing biomolecules, Angew. Chem. Int. Ed. 48 (2009) 4785–4787, https://doi.org/10.1002/anie.200901479.

[68] D.F. Báez, G. Ramos, A. Corvalán, M.L. Cordero, S. Bollo, M.J. Kogan, Effects of preparation on catalytic, magnetic and hybrid micromotors on their functional features and application in gastric cancer biomarker detection, Sensor. Actuator. B Chem. 310 (2020) 127843, https://doi.org/10.1016/j.snb.2020.127843.